

# Numerical Investigation on the Aerodynamic Design of Quadrotor Blades Operating in the Martian Atmosphere

Manuel Carreño Ruiz\*<sup>†</sup>, Francesco Bellelli\* and Domenic D'Ambrosio\*

\* Department of Mechanical and Aerospace Engineering, Politecnico di Torino

C.so Duca degli Abruzzi, 24, 10124 Torino, Italy

manuel.carreno@polito.it · s281612@studenti.polito.it · domenic.dambrosio@polito.it

<sup>†</sup>Corresponding author

## Abstract

The design of unmanned aerial systems (UAS) for flight in the Martian atmosphere is a relevant and current topic. The successful flight of the Ingenuity helicopter recently proved its applicability. In this paper, we discuss the aerodynamic optimization of airfoils and blades at ultra-low Reynolds number conditions. In particular, we focus on the efficient geometries revealed by different fidelity approaches and the sensitivity to geometrical parametrizations. In the case of airfoils, the performance predictions are carried out using unsteady CFD. We analyzed the influence of the Reynolds number on optimal geometries and proposed a globally efficient airfoil. We computed the polar of these airfoils to generate an aerodynamic database as they are necessary for rotor reduced-order models. We used the blade element method to generate efficient geometries employing a genetic algorithm and evaluated the resultant geometries with higher fidelity CFD simulations. Local thrust and torque distributions computed with different simulation approaches are compared. Finally, the blades are refined with an adjoint-based CFD optimization to produce a further improvement in performance.

## 1. Nomenclature

$C_Q = \frac{Q}{\rho\pi\Omega^2 R^5}$	=	rotor torque coefficient
$C_T = \frac{T}{\rho\pi\Omega^2 R^4}$	=	rotor thrust coefficient
$C_P = \frac{P}{\rho\pi\Omega^3 R^5}$	=	rotor power coefficient
$C_l = \frac{l}{\frac{1}{2}\rho V^2 c}$	=	airfoil lift coefficient
$C_d = \frac{d}{\frac{1}{2}\rho V^2 c}$	=	airfoil drag coefficient
$c$	=	airfoil chord
$V$	=	freestream velocity
$l$	=	airfoil lift
$d$	=	airfoil drag
$\Omega$	=	rotation rate in radians per second
$RPM$	=	rotation rate in revolutions per minute
$R$	=	rotor radius
$Re$	=	Reynolds number based on the chord
$M$	=	rotor tip Mach number
$T$	=	rotor thrust
$Q$	=	rotor torque
$P$	=	rotor power
$\rho$	=	air density
$\sigma = \frac{S_{rotor}}{A_{Disk}}$	=	rotor solidity

## 2. Introduction

The recent successful flights of Ingenuity on Mars have developed and increased interest in Martian exploration using Unmanned Aerial Systems(UAS). Flying on Mars is challenging due to different reasons. Despite Mars's gravity being about 38% of Earth's gravity, density is two orders of magnitude smaller than on Earth, which limits the capability of conventional rotors to develop enough thrust. The speed of sound on Mars is around 75% of the speed of sound on Earth at sea level. This fact limits the necessary increase in the rotation rate required to provide sufficient thrust due to transonic effects. High angular velocities will also cause an increase in torque which may result in larger motors and lead to motor heating issues. Low-density flight conditions are also found at high altitudes on Earth, with the added problem of higher gravity.

Several research studies have addressed, numerically and experimentally, the Ultra-low Reynolds number regime, which comprises Reynolds numbers ranging from 1,000 to 10,000. Kunz [14] performed extensive numerical work on efficient airfoils and rotors in these conditions. More recently, Koning [13, 12] and Bèzard [4, 3] presented detailed aerodynamic and optimization analyses of rotors in these conditions. Researchers from Japan have also pursued Martian flight publishing extensive and valuable experimental data obtained in the Martian Wind Tunnel at Tohoku University [16]. The authors have contributed to the study of this regime [9, 5], where we presented the first set of numerical simulations resulting in different efficient Martian blade designs. Being a very actual topic and considering that many space agencies are aiming to achieve Martian flight, it is rare to find well-documented efficient blade geometries and the optimization procedures employed to obtain them. The objective of this work is to discuss an efficient optimization strategy and present blade geometries that generates a thrust of 1.1 N with minimal power consumption. We present a 2 step hybrid fidelity approach. First, we design an efficient airfoil which then, which is used in the blade optimization loop.

For the 2D analysis, we performed compressible Navier-Stokes simulations using an unsteady laminar solver. We have included compressibility effects because the low-temperature conditions and small gas constant of the Martian atmosphere produce a low speed of sound. Add to this the high rotational velocity required to generate thrust in a low-density environment, resulting in a subsonic but high Mach number. For these simulations, we used the commercial Computational Fluid Dynamics (CFD) code STAR-CCM+, using its embedded Adjoint Navier-Stokes method to obtain optimal geometries for appropriate values of Mach and Reynolds numbers. We finally compared our optimized airfoils with other efficient geometries proposed in the literature [4, 12, 19] for similar operating conditions.

To design the three-dimensional blade geometry, we used two tools with different levels of fidelity. We started with the simple Blade Element Momentum Method (BEM), and we finished with a full Navier-Stokes simulation of the blades. We selected the best-performing geometries using an evolutionary algorithm (EA) to avoid local optimums, a common issue in rotor performance optimization due to the tight coupling between design and operating variables. Then, we used a gradient-based optimization approach to improve the solution. Reduced-order models are necessary, as optimization with full Navier-Stokes CFD simulations is computationally expensive. The optimal blades are evaluated with a Navier-Stokes simulation. Forces and moments are compared with those obtained with two reduced-order models, the BEM method and a Free Vortex Wake(FVW) method, to assess their prediction capabilities. Finally, we perform an adjoint-based CFD optimization to enhance the blade performance. The final blade is compared with previous designs shown in [5].

## 3. Airfoil Optimization

### 3.1 Efficient airfoils in ultra-low Reynolds number conditions.

Several researchers have studied airfoils in ultra-low Reynolds number conditions and have proposed optimal geometries. Kunz [14] presents optimal airfoils at different Reynolds numbers showing the strong dependency on optimal camber with Reynolds numbers. Optimal rotors found by different researchers [4, 5] do not present a constant Reynolds number, which is associated with a linear chord distribution. The Reynolds number changes with the radial coordinate, and so would the optimal airfoil required for each section in a 2D idealization. We can define two possible approaches for rotor design. The first would be to create blades with optimal airfoils at each radial station. The other possibility would be to create a globally optimal airfoil that performs well for different Reynolds numbers. Another aspect that influences the optimal airfoil shape is the range of angles of attack considered in the optimization. If only the angle of attack of maximum efficiency is considered, very aggressive geometries are obtained as shown in [5]. The geometry generated in this way, PoliTO-1, has a flat suction side when turned to the optimal angle of attack and concentrates the camber on the trailing edge, which folds downwards, forming a flap. The airfoil is very efficient at a reduced range of angles of attack close to the optimum, but outside this range, the boundary layer presents a strong leading-edge separation. On the other hand, when a range of angles of attack is considered in the optimization algorithm, the resultant airfoil has a balanced curvature distribution. When the leading edge is curved, separation is slightly delayed. An example of this geometry is proposed by Dessert [10, 4].

### 3.2 CFD adjoint-based optimization

We acknowledged that our previous geometry, PoliTO-1, was performing at low Reynolds and high angles of attack. This characteristic is related to the fact that the optimization was done for an initial angle of attack of 6 degrees and a Reynolds number of 3,000. To improve performance at low and intermediate angles of attack and higher Reynolds conditions, we performed an adjoint optimization starting with PoliTO-1 geometry rotated to 4 degrees and setting the Reynolds number at 10,000. The adjoint optimization uses a lattice of points placed with an offset to the surface to avoid excessive grid distortion and remeshing. We calculate the displacement of the control points used by the morpher with a steepest descend approach for each adjoint iteration, as shown in equation 2. The maximum displacement for each iteration is fixed to 0.5mm. The resultant geometry, PoliTO-2, is shown in figure 1, compared with other efficient airfoils presented in the literature for ultra-low Reynolds number conditions. It is clear how all the airfoils concentrate camber near the trailing edge, very different characteristics compared with conventional airfoils. PoliTO-2 presents a more even distribution of curvature than PoliTO-1 on the suction side, and the point of maximum curvature is not so close to the trailing edge. Figure 2 shows the aerodynamic efficiency of PoliTO-2 airfoil compared with PoliTO-1 and the airfoil proposed by Bézard[4]. We can appreciate how the efficiency of this airfoil outperforms both, PoliTO-1 and Bézard [4] geometries until a lift coefficient of 1.2 for all tested Reynolds number conditions. Considering that local lift coefficients in efficient rotors rarely go above 1.2, this airfoil should contribute to an enhanced performance of the rotor. The polar was computed for a Mach number of 0.5, which is the Mach number expected in the radial stations comprising 75%-90% of the blade, which is the most relevant region regarding thrust generation and power consumption. We extrapolated the polar to the rest of the radial stations using the Prandtl-Glauert transformation[11]. Considering that this transformation derives from the potential flow equation, it approximates well the variation in the lift coefficient induced by compressibility at these Reynolds numbers.

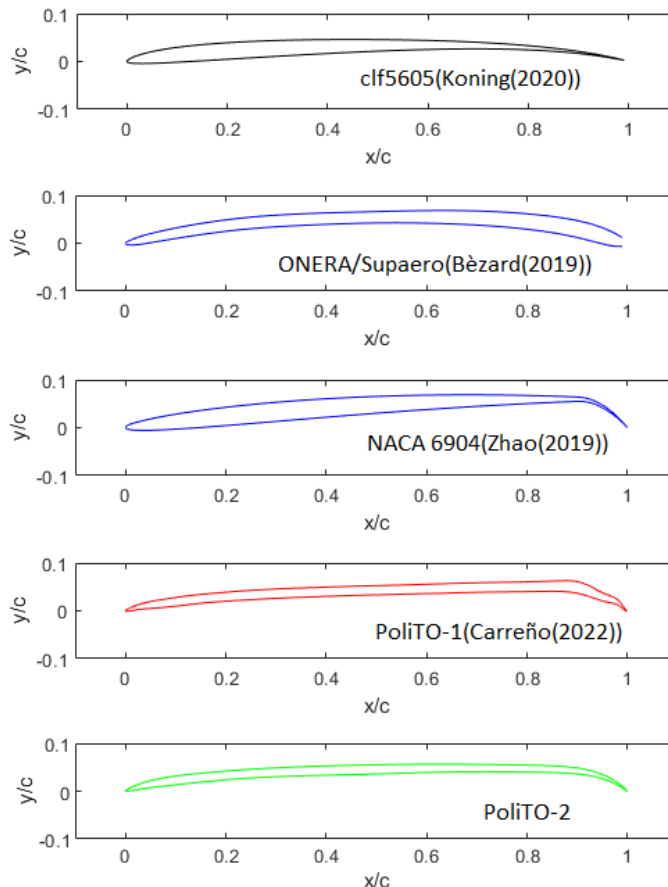


Figure 1: Airfoils reported in literature.

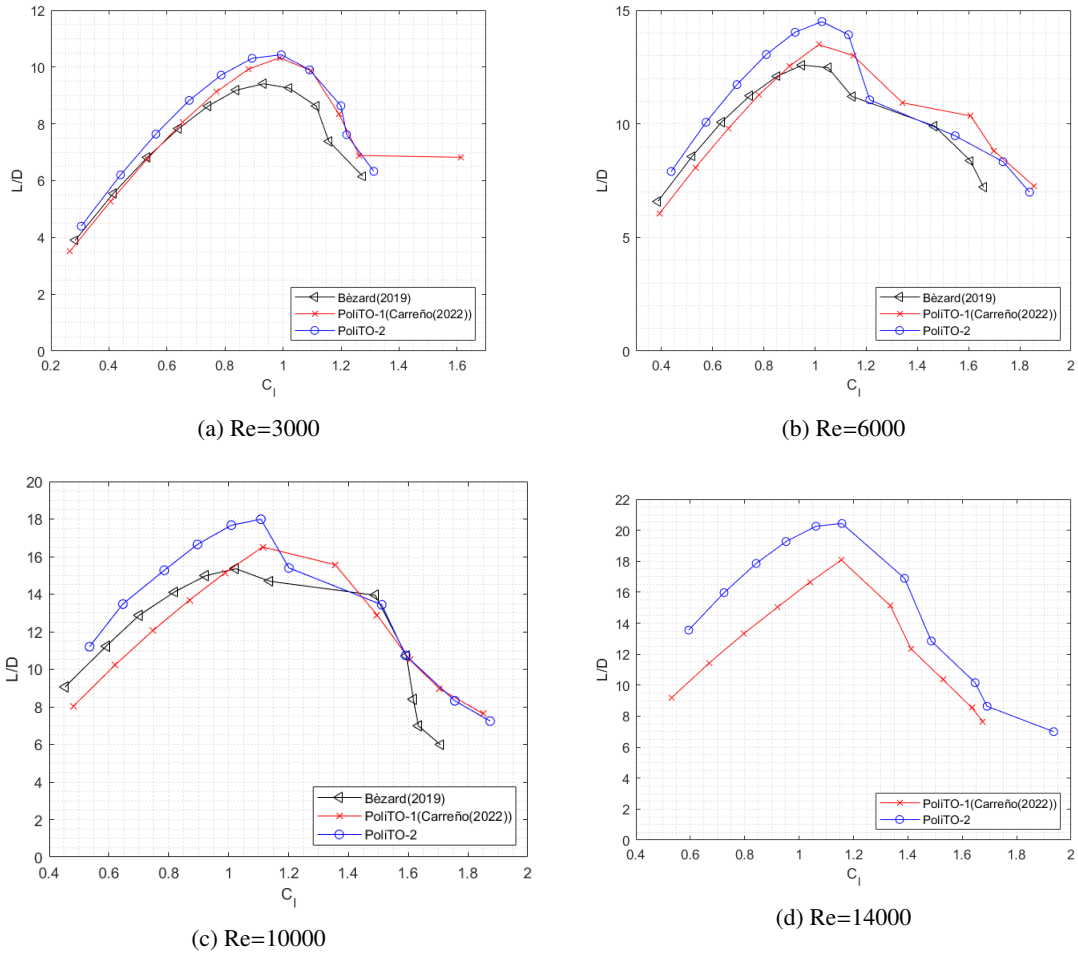


Figure 2: Comparison of aerodynamic efficiency at different Reynolds numbers: PoliTO1[5] vs Bézard(2019)[4] vs PoliTO-2. Data from [5] has been interpolated to the current Reynolds number.

#### 4. Blade Optimization

The present blade optimization consists of two steps. First, using a reduced order model, the BEM method is looped into a genetic algorithm, and then an adjoint CFD optimization is used to obtain an ulterior enhancement in performance. Figure 3 shows the optimization procedure. Our objective function is the power loading, including a penalization function to avoid the thrust dropping below 1.1N. We showed in a previous publication [5] how on Mars, it is mandatory to consider the mass of the blades in the optimization algorithm. If the mass is not penalized, the blades tend to have large chords near the root to compensate for the low Reynolds numbers. This fact deteriorates blade performance as the weight of the blade is not negligible compared to the thrust and reduces the available mass budget. We propose an optimization based on the power loading but calculating it using the net thrust, as defined in equation 1. This approach generates blades with a higher aspect ratio that rotate slightly faster. The standard power loading is slightly penalized, but the weight reduction compensates for the slight deterioration of the purely aerodynamic efficiency of the blade, which shows low sensitivity to the chord distribution after performing an adjoint refinement. This property suggests that any reasonable chord distribution can perform efficiently if twist distribution and rotation rate are accurately tuned. This finding is practical as the chord distribution could optimize the structural/mechanical performance of the blade and tune the twist and rotation rate to achieve satisfactory aerodynamic efficiencies. We used a milder mass penalization ( $\sigma = 0.5$ ) to avoid small chord distributions. In this way, we explore rotor aerodynamics for intermediate solidities that were not addressed in [5]. In the future, this implicit way to control chord distributions will be substituted with structural and mechanical constraints. The atmospheric conditions for our simulations are the average Mars atmospheric conditions reported in Bézard [3], a temperature of  $-63^{\circ}\text{C}$  and a pressure of 660 Pa. The atmosphere is idealized as pure carbon dioxide for the gas constant estimation in BEM simulations and as a fluid in CFD simulations.

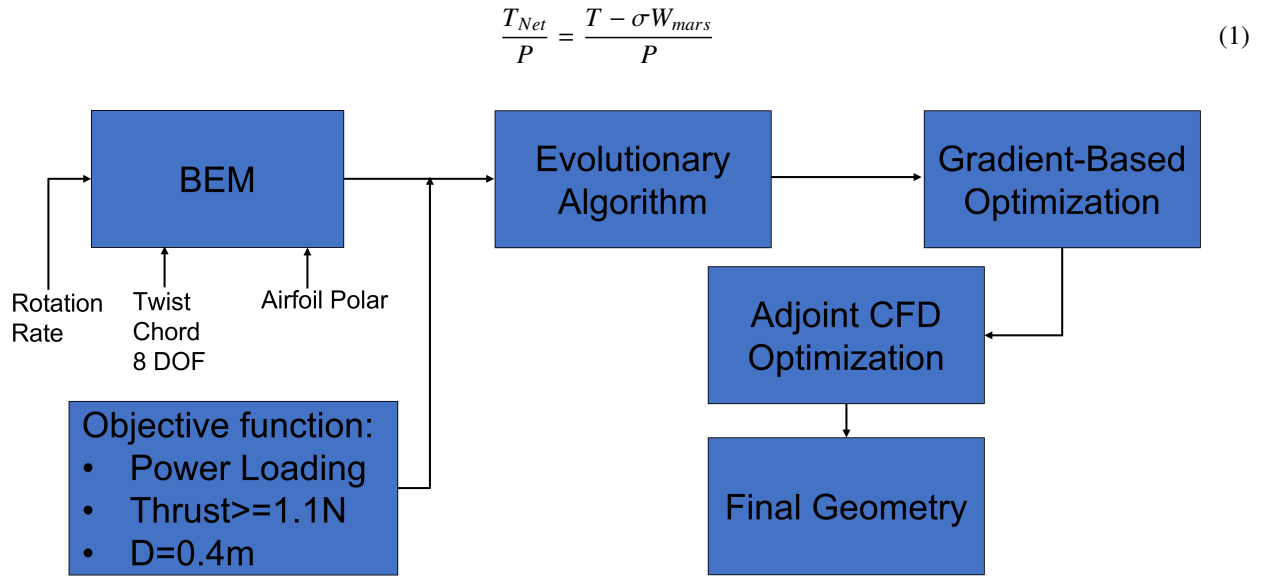


Figure 3: Optimization procedure

#### 4.1 BEM Optimization

The polar of the airfoil PoliTO-2 is computed for Reynolds number below 14,000 and angles of attack between 0 and 10 degrees. We interpolate these values using Akima splines[1] for both Reynolds numbers and angles of attack to ensure a continuous function necessary for the BEM algorithm to converge. This paper presents a blade parametrization that uses Akima splines with 4 degrees of freedom for the chord distribution and 4 degrees of freedom for the twist distribution. The rotation rate is also considered a design variable and is limited to avoid tip Mach numbers above 0.7. An in-house BEM solver [6, 17, 15] is used due to the compromise between accuracy and computational cost. A previous publication [6] shows how a more sophisticated free vortex wake method enhances the prediction of inflow angles compared with BEM simulations. This finding is in line with Bézard [4]. However, the computational cost of the free vortex wake method is a couple of orders of magnitude larger than the blade element momentum method. Considering that we will perform an adjoint refinement, we decided to use the blade element method in the evolutionary algorithm. The evolutionary algorithm uses a roulette approach for the selection function and a rank fitness scaling. A 5% of elite members avoid the loss of performing geometries after the cross-over and mutation steps. The algorithm uses an initial population of 200 members and evolves for 200 generations. The optimal geometry undergoes an ulterior refinement process employing a gradient-based approach. Figure 4 shows the optimal geometry. We can appreciate an almost constant chord distribution. Figure 5 shows the radial distribution of the most relevant quantities predicted by the BEM for the optimal blade. We appreciate how the lift coefficient value matches well the angle of maximum efficiency as shown in figure 2.

#### 4.2 Navier-Stokes Evaluation of the blades

To check the results obtained with the BEM model, we performed laminar simulations of the blades using the commercial CFD software STAR-CCM+ [18]. The maximum Reynolds number for their specified rotational speed is 14,000 at a radial position of 16 cm for the 2-bladed rotor, as shown in figure 6b. At the higher Reynolds numbers of this regime, separation-induced transition may be present on the blade sections. However, the flow remains attached until the trailing edge and, therefore, transition to turbulence will occur on the wake making its impact on performance would be relatively small. In this paper, we will work under the assumption that Navier-Stokes equations are a reliable mathematical model to predict rotors' performance in Mars atmosphere, as shown in [4].

We validated the laminar solver of STARCCM+ in a previous publication [9] by comparing CFD simulations with experimental results presented by Munday [16]. The latter refers to an experimental campaign at the Martian Wind Tunnel (MWT) of Tohoku University on a triangular wing invested by a current at ultra-low Reynolds numbers. The grids for the rotor simulations presented in this paper contain approximately 12 million cells. We used a sliding grid approach with a second-order discretization, a second-order implicit time-dependent scheme and a time step equivalent to a blade rotation of 1 degree. Ten rotor revolutions are sufficient for thrust and torque convergence.

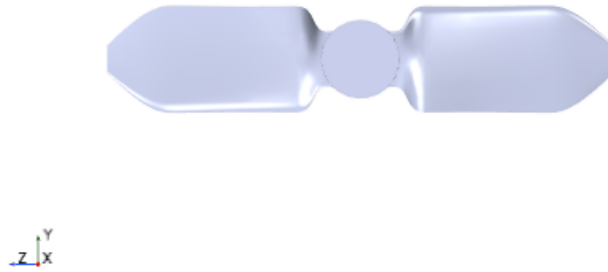


Figure 4: BEM optimal geometry.

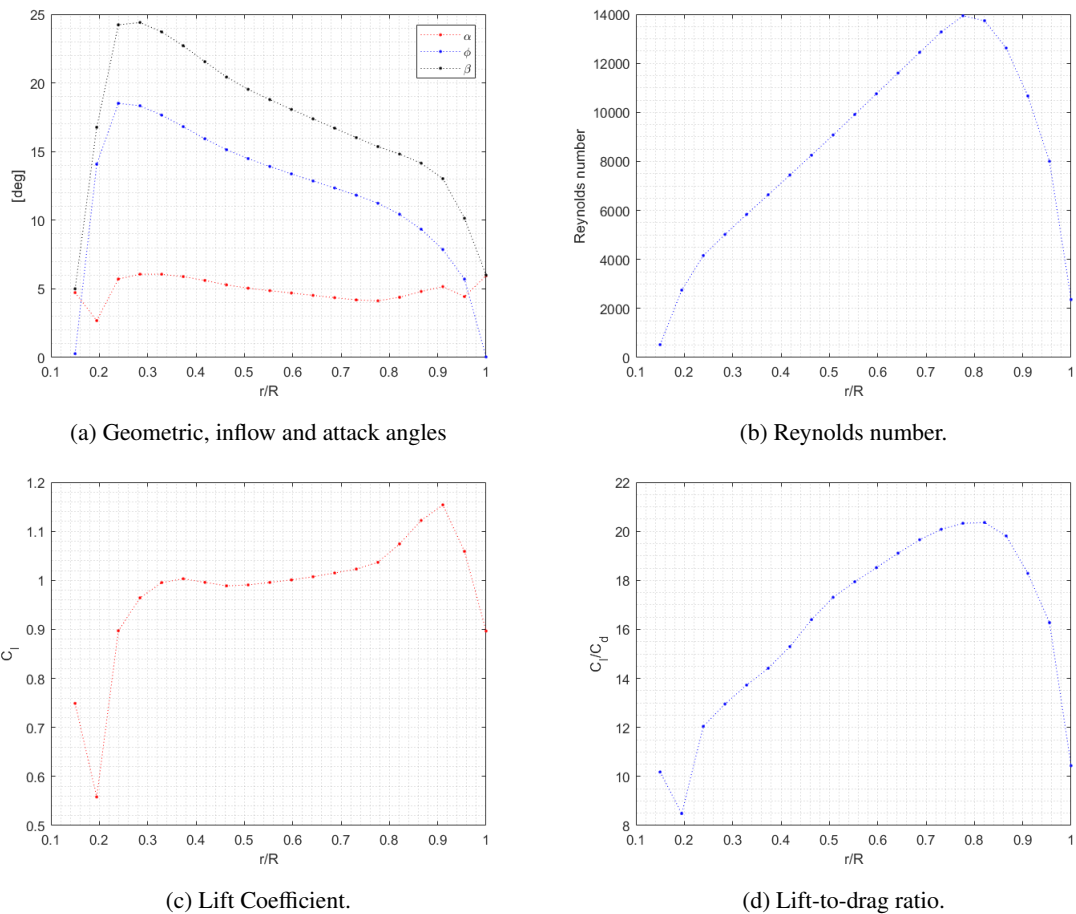


Figure 5: BEM local results on the optimal geometry.

Table 1 shows the comparison between CFD, BEM and Non-Linear Lifting Line Free Vortex Wake(NLL-FVW) evaluations of the blade. We used an in-house NLL-FVW code validated and verified in [2, 6] for a conventional rotor working in very-low Reynolds number conditions. The NLL-FVW code reveals a slight over-prediction of thrust compared to both CFD and BEM codes. Figure 6 shows an overall good agreement of torque and thrust radial distributions between all solvers with both reduced-order models overestimating the maximum thrust and torque values. Figure 7 shows the Q-criterion of the optimized blade. we can see how the tip vortex passes near the blade which will affect the induced

Table 1: Optimal BEM geometry performance with different solvers.

Solver	Omega(rpm)	Thrust(N)	Torque(Nm)	T/P (N/W)
BEM	6588	1.10	0.0414	0.0385
CFD	6588	1.046	0.0425	0.0357
NLL-FVW	6588	1.14	0.0410	0.0403
CFD	6755	1.10	0.0447	0.0348

angles. It is especially in these regions where the BEM solver fails to predict the flow due to its lack of explicit wake modelling as both the free vortex wake does. However, we do not appreciate a clear improvement in the predictions performed by the NLL-FVW code which fails to model the near tip region for these Ultra-low Reynolds numbers. Considering that the computational cost of one blade evaluation using the BEM code (1 second) is a couple of orders of magnitude lower compared to the NLL-FVW approach (10 minutes) and the limited improvement, if any, on the aerodynamic predictions, made us chose the BEM model as our solver to embed into the optimization process. In any case, the discrepancies in the induction prediction with the reduced-order models are expected to be corrected with the adjoint refinement performed in the following section.

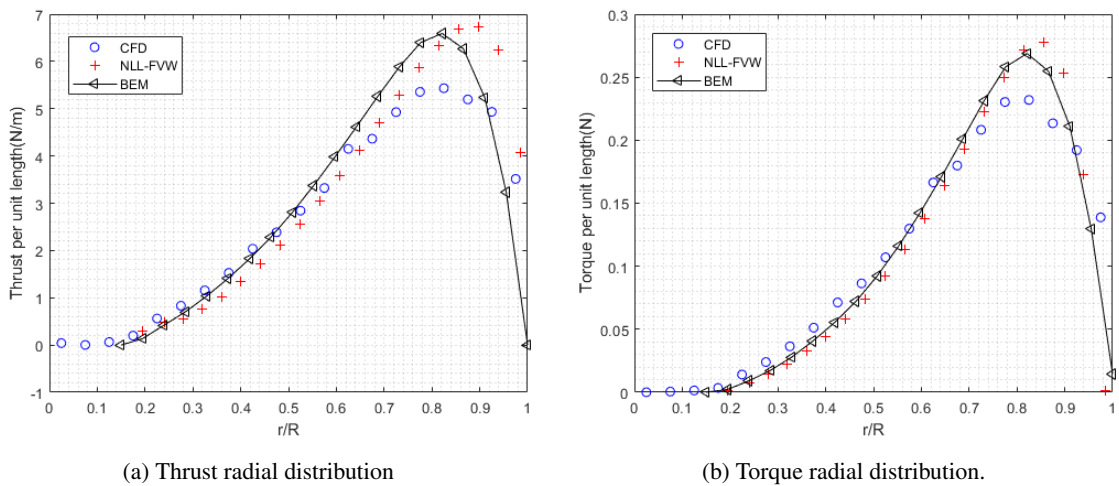


Figure 6: Local forces and moments on the blade predicted by different solvers.

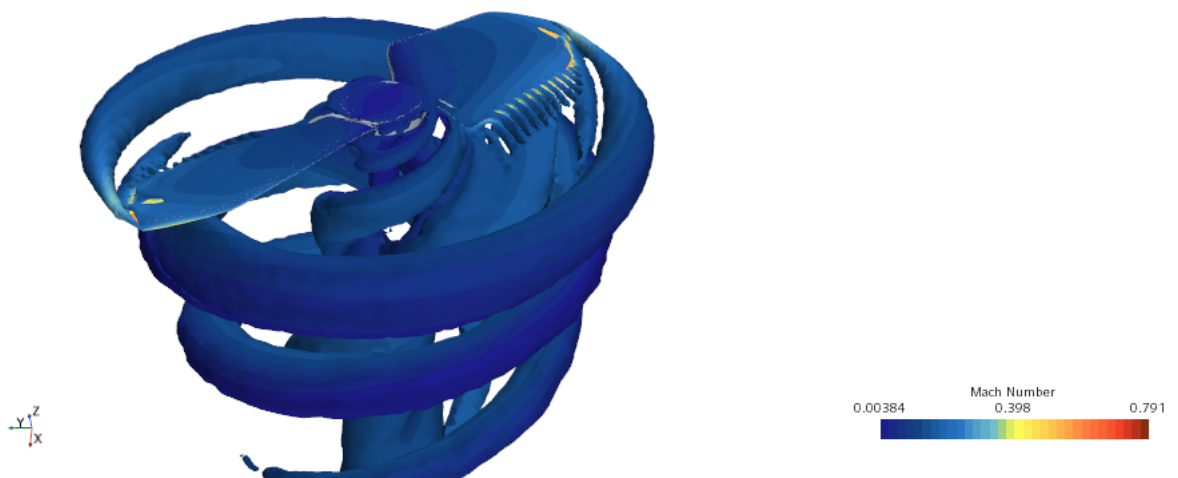


Figure 7: Q-criterion iso-surface colored with Mach Number obtained with unsteady solver for BEM optimal geometry.

### 4.3 Adjoint-based optimization

We carried out another optimization activity to account for the three-dimensional effects that the initial BEM optimization might have neglected. The Adjoint flow solver in STAR-CCM+ is only available for the steady solver. However, we showed in [7, 15, 8] that steady-state calculations using a Moving Reference Frame (MRF) approach provide results that are comparable to the unsteady sliding mesh approach. However, the steady solver does not capture the effect of vortex emission from the trailing edge seen in the unsteady simulations, which generally improves the blade performance. The overall consistency between steady and unsteady solutions suggests that an optimal shape obtained using steady-state simulations will also enhance the performance in time-dependent conditions. These simulations include a periodic boundary condition that allows the simulation of only one blade. The grid, in this case, is around 6 million cells. In this case, the choice of the objective function is critical as the power loading rises for lower thrust values. To maintain adequate thrust values and improve power loading, we propose an objective function which multiplies the power loading by the square root of the thrust. This choice allows us to perform optimizations at a constant rotation rate. The angular velocity is then adjusted to match the thrust restriction. The grid sensitivities with respect to the objective function allow us to find the direction in which morphing the mesh provides an increase in efficiency. A steepest descent approach is employed, limiting the maximum displacements of the control points to 0.5 mm for each adjoint iteration. Figure 8 shows the lattice of points that the morpher uses to deform the grid. We can appreciate how after the first iteration, adjoint sensitivities to the objective function suggest reducing trailing edge curvature and reducing the angle of attack in the 75%-90% radial coordinate region. Figure 9 shows the final disposition of the blades. We can identify how towards the tip, where Reynolds numbers are larger, the airfoil geometry reduces curvature in the leading edge and redistributes it evenly throughout the chord. The angle of attack is reduced in all the blade span except in the vicinity of the tip region. To compare the performance of the final blade geometry, we performed a full unsteady Navier-Stokes evaluation with the same grid settings as the one used to evaluate the BEM geometry. Table 2 shows how the adjoint performs an ulterior improvement of the blade performance. It is interesting to note how the improvement in this case, around 5%, is considerably lower compared to that found in our previous publication [5]. The authors believe that this reduction in improvement is caused by the less aggressive and more efficient initial airfoil geometry. The original BEM geometry seems to be already performing, which is a huge advantage, considering the low computational costs of BEM simulations. The power consumed by this blade at a thrust level of 1.1 N is 30.12 W, around 1.5% lower than the most efficient blade reported in [5]. This improvement is obtained despite having a smaller solidity which generally deteriorates performance due to the lowered Reynolds number. We believe that the increase in performance following an equivalent procedure is associated with the improved airfoil geometry PoliTO-2 that we use in the generation of this blade. Another possible reason for this improvement is that this geometry does not present a leading-edge vortex as seen in larger solidity rotors presented in previous Martian rotor publications [4, 3, 5].

$$D_i = D_{i-1} + \frac{h_{step} \nabla f}{\max(|\nabla f|)} \quad (2)$$

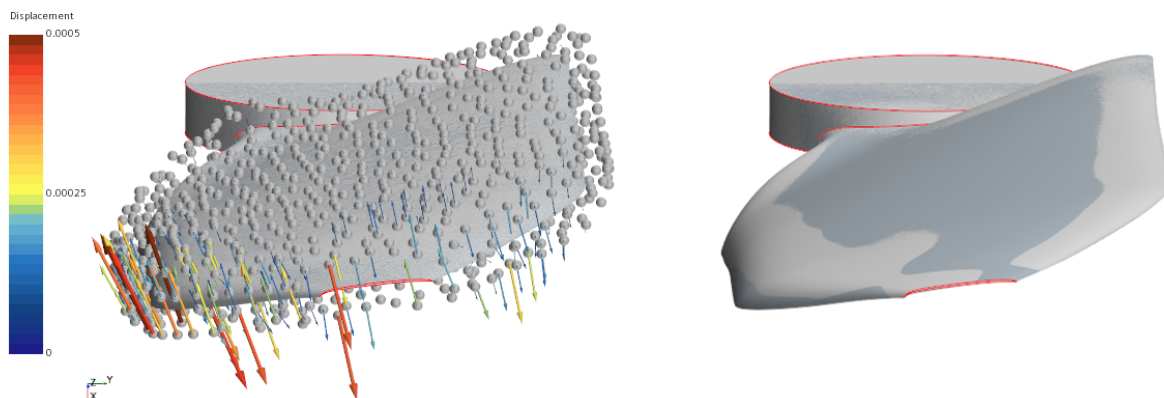


Figure 8: Morpher control point displacements after first adjoint iteration(Left). Comparison between original(Light grey) and morphed surface(Dark Grey) after first adjoint iteration(Right).



Figure 9: Comparison between original(Light grey) and morphed surface(Dark Grey) after the final adjoint iteration.

Table 2: Comparison between BEM and CFD-Adjoint optimal geometries.

<b>Geometry-Solver</b>	<b>Omega(rpm)</b>	<b>Thrust(N)</b>	<b>Torque(Nm)</b>	<b>P (W)</b>
BEM-CFD	6755	1.10	0.0447	31.62
Adjoint-CFD	7096	1.10	0.0405	30.12
Difference(%)	5.0	0	-9.4	-4.7

## 5. Conclusions

The multi-fidelity optimization procedure described in this paper provides aerodynamically efficient rotors. The presented approach is divided into two steps, an airfoil 2-dimensional optimization followed by a 3-dimensional rotor optimization. The combination of different fidelity solvers allows us to generate rotor geometries in a fast and accurate manner. The mix of gradient-based and evolutionary optimization strategies permits the exploration of different local optima and exploits them to obtain the most efficient geometry. The optimal airfoil geometry presented in this paper, PoliTO-2, optimized for a Reynolds number of 10,000, outperforms our previous geometry, PoliTO-1, which was optimized for a Reynolds number of 3000 and other airfoils found in the literature. The improvement in the efficiency of the airfoil reflects positively on the performance of the final blades compared to previous designs, as it provides an initial geometry closer to the actual optimum. The BEM solver provides satisfactory predictions which are sufficient for the generation of blade geometries which perform efficiently according to CFD simulations. The CFD adjoint-based optimization on this geometry produces an ulterior improvement in performance. The improvement, in this case, is smaller than in previous optimizations possibly, due to the more efficient airfoil present in the initial geometry. In any case, the presented outperforms all the blades that were presented in previous publications using this optimization approach. This fact is possibly due to a relatively large solidity without triggering a leading-edge vortex formation.

Future work will address a thorough optimization of the chord distributions, including structural/mechanical restrictions, which are necessary to generate efficient yet practically feasible blade designs.

## References

- [1] Hiroshi Akima. A new method of interpolation and smooth curve fitting based on local procedures. *Journal of the ACM (JACM)*, 17(4):589–602, 1970.
- [2] Mario Ali. Development and validation of a reduced order method for the study of flow on a rotor. Master's thesis, Politecnico di Torino, 2021.

- [3] Hervé Bézard, Thibault Désert, Thierry Jardin, and Jean-Marc Moschetta. Numerical and experimental aerodynamic investigation of a micro-uav for flying on mars. In *76th Annual Forum & Technology Display*, 2020.
- [4] Hervé Bézard, Thibault Desert, Jean-Marc Moschetta, and Thierry Jardin. Aerodynamic design of a Martian micro air vehicle. In *EUCASS 2019*, MADRID, Spain, July 2019.
- [5] Manuel Carreño Ruiz and Domenic D’Ambrosio. Aerodynamic optimization of quadrotor blades operating in the martian atmosphere. In *AIAA 2022 SCITECH*, 2022.
- [6] Manuel Carreño Ruiz, Andrea Manavella, and Domenic D’Ambrosio. Numerical and experimental validation and comparison of reduced order models for small scale rotor hovering performance prediction. In *AIAA 2022 SCITECH*, 2022.
- [7] Manuel Carreño Ruiz, Matteo Scanavino, Domenic D’Ambrosio, Giorgio Guglieri, and Andrea Vilardi. Experimental and numerical analysis of multicopter rotor aerodynamics. In *AIAA Aviation 2021 Forum*, 2021.
- [8] Manuel Carreño Ruiz. Cfd simulation of propellers: Best practices analysis. Master’s thesis, Politecnico di Torino, 2019.
- [9] Manuel Carreño Ruiz and Domenic D’Ambrosio. Validation and application of aerodynamic simulations in the martian atmosphere. In *26th Conference of the Italian Association of Aeronautics and Astronautics-AIDAA 2021*, 2021.
- [10] Thibault Desert, Jean-Marc Moschetta, and Hervé Bézard. Numerical and experimental investigation of an airfoil design for a martian micro rotorcraft. *International Journal of Micro Air Vehicles*, 10(3):262–272, 2018.
- [11] Hermann Glauert. The effect of compressibility on the lift of an aerofoil. *Proceedings of the Royal Society of London. Series A, Containing Papers of a Mathematical and Physical Character*, 118(779):113–119, 1928.
- [12] Witold J Koning, Ethan A Romander, and Wayne Johnson. Optimization of low reynolds number airfoils for martian rotor applications using an evolutionary algorithm. In *AIAA Scitech 2020 Forum*, page 0084, 2020.
- [13] Witold JF Koning, Wayne Johnson, and Brian G Allan. Generation of mars helicopter rotor model for comprehensive analyses. *AHS Aeromechanics Design for Transformative Vertical Flight*, 2018.
- [14] Peter J Kunz. *Aerodynamics and design for ultra-low Reynolds number flight*. PhD thesis, Standford University, 2003.
- [15] Andrea Manavella. Low reynolds number propeller performance validation by cfd analysis and reduced order models. Master’s thesis, Politecnico di Torino, 2021.
- [16] Phillip M Munday, Kunihiko Taira, Tetsuya Suwa, Daiju Numata, and Keisuke Asai. Nonlinear lift on a triangular airfoil in low-reynolds-number compressible flow. *Journal of Aircraft*, 52(3):924–931, 2015.
- [17] Matteo Scanavino. *Design and testing methodologies for UAVs under extreme environmental conditions*. PhD thesis, Politecnico di Torino, 2021.
- [18] Siemens Digital Industries Software. Simcenter STAR-CCM+ User Guide v. 2019.3, Siemens 2019.
- [19] Pengyue Zhao, Qiquan Quan, Shuitian Chen, Dewei Tang, and Zongquan Deng. Experimental investigation on hover performance of a single-rotor system for mars helicopter. *Aerospace Science and Technology*, 86:582–591, 2019.